



HAL
open science

NADPH oxidase (NOX) isoforms are inhibited by celastrol with a dual mode of action

Vincent Jaquet, Julien Marcoux, Eric Forest, Kevin Leidal, Sally McCormick,
Yvonne Westermaier, Remo Perozzo, Olivier Plastre, Laetitia Fioraso-cartier,
Becky Diebold, et al.

► **To cite this version:**

Vincent Jaquet, Julien Marcoux, Eric Forest, Kevin Leidal, Sally McCormick, et al.. NADPH oxidase (NOX) isoforms are inhibited by celastrol with a dual mode of action. *British Journal of Pharmacology*, 2011, 164 (2b), pp.507-520. 10.1111/j.1476-5381.2011.01439.x . hal-02335573

HAL Id: hal-02335573

<https://hal.science/hal-02335573>

Submitted on 19 Mar 2021

HAL is a multi-disciplinary open access archive for the deposit and dissemination of scientific research documents, whether they are published or not. The documents may come from teaching and research institutions in France or abroad, or from public or private research centers.

L'archive ouverte pluridisciplinaire **HAL**, est destinée au dépôt et à la diffusion de documents scientifiques de niveau recherche, publiés ou non, émanant des établissements d'enseignement et de recherche français ou étrangers, des laboratoires publics ou privés.

RESEARCH PAPER

NADPH oxidase (NOX) isoforms are inhibited by celastrol with a dual mode of action

Vincent Jaquet¹, Julien Marcoux^{2,3}, Eric Forest³, Kevin G Leidal⁴, Sally McCormick⁴, Yvonne Westermaier⁵, Remo Perozzo⁵, Olivier Plastre¹, Laetitia Fioraso-Cartier¹, Becky Diebold⁶, Leonardo Scapozza⁵, William M Nauseef⁴, Franck Fieschi⁷, Karl-Heinz Krause^{1,8*} and Karen Bedard^{9*}

¹Department of Pathology and Immunology, Centre Médical Universitaire, Geneva, Switzerland, ²Laboratoire des Protéines Membranaires CEA, DSV, Institut de Biologie Structurale (IBS), Grenoble, France, ³Laboratoire de Spectrométrie de Masse des Protéines, CEA, DSV, Institut de Biologie Structurale (IBS), Grenoble, France, ⁴Inflammation Program and Department of Medicine, Roy J and Lucille A. Carver College of Medicine, University of Iowa, Coralville, IA and the Veterans Administration Medical Center, Iowa City, IA, USA ⁵Pharmaceutical Biochemistry Group, School of Pharmaceutical Sciences, University of Geneva, Geneva, Switzerland, ⁶Department of Pathology, Emory University, Atlanta, GA, USA, ⁷Membrane & Pathogens Group, Institut de Biologie Structurale (IBS), Université Joseph Fourier and Institut Universitaire de France, Grenoble, France, ⁸Department of Genetic and Laboratory Medicine, Geneva University Hospitals, Geneva, Switzerland, ⁹Department of Pathology, Sir Charles Tupper Medical Building, Dalhousie University, Halifax, Nova Scotia, Canada

Correspondence

Vincent Jaquet, Department of Pathology and Immunology, Centre Médical Universitaire, 1 rue Michel-Servet, 1211 Geneva 4, Switzerland. E-mail: vincent.jaquet@unige.ch

*These authors contributed equally.

Keywords

reactive oxygen species; celastrol; NADPH oxidase; NOX inhibitor; SH3 domain; *Tripterygium wilfordii* Hook F.

Received

16 November 2010

Revised

18 February 2011

Accepted

17 March 2011

BACKGROUND

Celastrol is one of several bioactive compounds extracted from the medicinal plant *Tripterygium wilfordii*. Celastrol is used to treat inflammatory conditions, and shows benefits in models of neurodegenerative disease, cancer and arthritis, although its mechanism of action is incompletely understood.

EXPERIMENTAL APPROACH

Celastrol was tested on human NADPH oxidases (NOXs) using a panel of experiments: production of reactive oxygen species and oxygen consumption by NOX enzymes, xanthine oxidase activity, cell toxicity, phagocyte oxidase subunit translocation, and binding to cytosolic subunits of NOX enzymes. The effect of celastrol was compared with diphenyleneiodonium, an established inhibitor of flavoproteins.

KEY RESULTS

Low concentrations of celastrol completely inhibited NOX1, NOX2, NOX4 and NOX5 within minutes with concentration–response curves exhibiting higher Hill coefficients and lower IC₅₀ values for NOX1 and NOX2 compared with NOX4 and NOX5, suggesting differences in their mode of action. In a cell-free system, celastrol had an IC₅₀ of 1.24 and 8.4 μM for NOX2 and NOX5, respectively. Cytotoxicity, oxidant scavenging, and inhibition of p47^{phox} translocation could not account for NOX inhibition. Celastrol bound to a recombinant p47^{phox} and disrupted the binding of the proline rich region of p22^{phox} to the tandem SH3 domain of p47^{phox} and NOXO1, the cytosolic subunits of NOX2 and NOX1, respectively.

CONCLUSIONS AND IMPLICATIONS

These results demonstrate that celastrol is a potent inhibitor of NOX enzymes in general with increased potency against NOX1 and NOX2. Furthermore, inhibition of NOX1 and NOX2 was mediated via a novel mode of action, namely inhibition of a functional association between cytosolic subunits and the membrane flavocytochrome.

Abbreviations

BAPTA, 1,2-bis(2-aminophenoxy)ethane-N,N,N',N'-tetraacetic acid; DMEM, Dulbecco's modified Eagle medium; DTT, dithiothreitol; DPI, diphenyleneiodonium; FBS, fetal bovine serum; GST, glutathione-S-transferase; IPTG, isopropyl-1-thio- β -D-galactopyranoside; MCLA, 2-methyl-6-(4-methoxyphenyl)-3,7-dihydroimidazo[1,2-a]pyrazin-3(7H)-1 hydrochloride; NADPH, nicotinamide adenine dinucleotide phosphate; NOX, NADPH oxidase; NOXO1, NADPH oxidase organiser type 1; PMA, phorbol myristate acetate; RPMI, Roswell Park Memorial Institute; ROS, reactive oxygen species; SH3, src homology domain 3; SOD, superoxide dismutase

Introduction

Extracts of the plant *Tripterygium wilfordii* Hook F. of the *Celastraceae* family are used in Chinese traditional medicine to treat chronic inflammation and autoimmune diseases, and have clinical efficacy in rheumatoid arthritis (Tao *et al.*, 1989). In patients undergoing kidney transplantation, daily oral intake of *Tripterygium wilfordii* extracts in addition to immunosuppressive therapy reduces allograft rejection and increases long-term allograft survival (Ji *et al.*, 2006). Although the major active component of the extracts is believed to be triptolide, another component, celastrol, is also biologically active. Celastrol (molecular weight 450 kDa) is an orange-coloured triterpene containing an acidic group on one end and a phenolic quinone at the other end. It has a protective effect in inflammatory and autoimmune conditions, cancer and fertility (for review, see Brinker *et al.*, 2007). Celastrol also has a positive effect in several different models of CNS degenerative diseases that are characterized by an overproduction of reactive oxygen species (ROS), such as amyotrophic lateral sclerosis (Kiaei *et al.*, 2005), Huntington's disease (Wang *et al.*, 2005) and Parkinson's disease (Cleren *et al.*, 2005). However, the precise mechanisms by which celastrol achieves these benefits is not fully known.

The NOX enzymes are a family of ROS-generating nicotinamide adenine dinucleotide phosphate (NADPH) oxidases (NOX) comprising seven members (NOX1, NOX2, NOX3, NOX4, NOX5, DUOX1 and DUOX2). All NOX isoforms function as electron transporters and catalyse the reduction of molecular oxygen to generate the superoxide anion. Whereas NOX enzymes are expressed throughout the body, each isoform possesses a unique pattern of tissue and subcellular distribution and there is little redundancy among NOX isoforms. The role of NOX enzymes in oxidative stress-related pathologies is increasingly recognized, in particular for cardiovascular and neurodegenerative diseases, and they represent a promising pharmacological target (Lambeth *et al.*, 2008).

Despite their similar core structures, NOX isoforms have different mechanisms of activation. NOX1, NOX2 and NOX3 require association with cytosolic components [p47^{phox}, p67^{phox}, NOXO1 (NOX organizer type 1), NOXA1 (NOX activator type 1)], NOX4 is constitutively active, and NOX5 and DUOXes are activated by an elevation in intracellular Ca²⁺. The activation mechanism for NOX2, the enzyme responsible for the oxidative burst of phagocytes, is well defined: upon activation, p47^{phox} is phosphorylated and translocates to the membrane through the formation of a complex with p67^{phox} and p40^{phox}. Phosphorylation of p47^{phox} induces a conformational change in a tandem src homology (SH3) domain that

enables binding to a proline-rich region in the cytosolic C-terminus of the transmembrane subunit p22^{phox}. Independently, the GTP binding protein Rac also moves to the membrane and activation occurs (reviewed in Bedard and Krause, 2007).

During a screen using a NINDS (National Institute of Neurological Disorders and Stroke) library (data not shown), we observed that celastrol inhibited luminol-enhanced luminescence mediated by NOX2 in neutrophils activated by the phorbol ester phorbol myristate acetate (PMA). In order to confirm that the decrease in ROS generation observed in the NINDS screen was due to NOX inhibition, we used a palette of assays (Jaquet *et al.*, 2009) to demonstrate a direct effect of celastrol on NOX enzymes and to exclude the possibility that the reduction in ROS was due to off-target effects such as a ROS scavenging action or toxicity. In this study, we demonstrated that celastrol, like the flavoprotein inhibitor diphenyleneiodonium (DPI), rapidly inhibited NOX1, NOX2, NOX4 and NOX5 in a concentration-dependent way. However, unlike DPI, celastrol showed positive co-operative inhibition on NOX1 and NOX2 compared with its effects on NOX4 and NOX5, and had less of an effect on xanthine oxidase. We propose that this selective co-operative inhibition of NOX1 and NOX2 reflects the subunit-dependent nature of these isoforms, as demonstrated by the finding that celastrol specifically bound to p47^{phox} and disrupted the binding of p22^{phox} to the tandem SH3 domain of NOXO1 and p47^{phox}, a novel mechanism for inhibiting NOX enzyme activity.

Methods

Cells

Human neutrophils were isolated from fresh whole blood collected from healthy volunteers (Nauseef, 2007). Briefly, blood was collected in sodium citrate (3.8%), and sedimented with dextran sulphate (4%) in saline. Cells pelleted from the supernatant were resuspended in PBS and separated through Ficoll Plaque™ Plus (Amersham Biosciences AB, Uppsala, Sweden). Remaining red blood cells were hypotonically lysed, and isolated neutrophils were washed and resuspended in Hank's buffered salt solution (HBSS) and kept on ice. PLB-985 myeloid cells were cultured in Roswell Park Memorial Institute (RPMI) medium supplemented with FBS (10%), penicillin (100 U·mL⁻¹) and streptomycin (100 μ g·mL⁻¹) and grown at 37°C in air with 5% CO₂. The cells were differentiated into granulocyte-like cells by the addition of dimethyl sulphoxide (DMSO) (1.25%) to the medium for 3–5 days.

HEK293T cells expressing tetracycline-inducible human NOX4 and HEK293 cells stably expressing human NOX5 were generated as described previously (Serrander *et al.*, 2007a,b). HEK cells were cultured in Dulbecco's modified Eagle medium (DMEM) with 4.5 g·L⁻¹ glucose, supplemented with FBS (10%), penicillin (100 U·mL⁻¹) and streptomycin (100 µg·mL⁻¹) at 37°C in air with 5% CO₂.

CHO cells were modified to stably express human NOX1, NOXO1, NOXA1 and p22^{phox} by amplifying the full length sequences from cDNA with Gateway (Invitrogen) adaptable primers. In a two-step process, the sequences were inserted first into pDONR 221 (Invitrogen), and then subcloned into 2K7 vectors (Suter *et al.*, 2006) with the cytomegalovirus promoter. The vectors for NOX1, NOXO1, NOXA1 and p22^{phox} contained green fluorescence protein, zeocin resistance, neomycin resistance and blasticidin resistance, respectively, as a means of selection. A monoclonal cell line was generated through a limiting dilution series in a 96 well plate. CHO cells were cultured in DMEM F12 medium (DMEM/F12) (1:1) supplemented with FBS (10%), penicillin (100 U·mL⁻¹) and streptomycin (100 µg·mL⁻¹) at 37°C in air with 5% CO₂.

Membrane preparation

Isolated human neutrophils or HEK293 expressing human NOX5 (approximately 10⁷ cells) were suspended in 1.5 mL of a sonication buffer containing PBS (0.1 X), sucrose (11%), NaCl (120 mM) and EGTA (1 mM) supplemented with protease inhibitors (Complete Mini, Roche) and sonicated two times for 45 s (level 4, Brandon Sonifier 250). Cell debris were removed by 10 min centrifugation at 800×g. The supernatant was laid on a sucrose gradient consisting of a bottom layer of 1.5 mL sucrose (40%) and an upper layer of 1.5 mL sucrose (17%). Ultracentrifugation was performed at 150 000×g in a SW60 rotor for 30 min at 4°C. Following separation, the upper cytosolic fraction was discarded and the cloudy membrane fraction was kept, protein content was measured using standard Bradford procedure and was stored in small aliquots at -80°C.

ROS measurement by Amplex Red

The production of hydrogen peroxide by NOX in intact cells was measured using Amplex Red (Molecular Probes) fluorescence using FluoSTAR OPTIMA, BMG labtech. Cells were collected by trypsinization for adherent cells (CHO, HEK) or centrifugation for cells in suspension (PLB-985, human neutrophils), washed with HBSS, counted and resuspended in HBSS at 500 000 cells·mL⁻¹. Cells were seeded in 96-well plates at a density of 50 000 cells (100 µL). Inhibitors were added to the cells for 10 min, and then the Amplex Red reaction mixture was added to give final concentrations of 0.005 U·mL⁻¹ horseradish peroxidase and 25 µM Amplex Red.

Cells were pre-incubated with the inhibitors for 10 min before measurement. Where indicated, NOX1 and NOX2 were activated with the PKC activator PMA (0.1 µM), and NOX5 was activated with the Ca²⁺ ionophore ionomycin (1 µM). Tetracycline (1 µg·mL⁻¹) was added to the medium of tetracycline-inducible HEK-NOX4 cells for 18 h before measurement. Fluorescence was recorded for 30–60 min at 37°C with excitation and emission wavelengths of 550 nm and 600 nm respectively. The amount of ROS generated was cal-

culated from a hydrogen peroxide standard curve ranging from 5 µM to 0.156 µM, which was included on each plate. The generation of hydrogen peroxide by the xanthine/xanthine oxidase was performed in PBS supplemented with xanthine oxidase (0.004 U), ethylenediaminetetraacetic acid (EDTA) (0.3 mM), HRP (0.005 U·mL⁻¹) and Amplex Red 0.025 mM. The reaction was started by the addition of xanthine (0.5 mM). Fluorescence of each well was measured at 37°C for 15 min. The increase in fluorescence (AUF min⁻¹) was calculated.

ROS measurement by MCLA luminescence

In the cell-free membrane systems, superoxide generation was measured with the 2-methyl-6-(4-methoxyphenyl)-3,7-dihydroimidazo[1,2-a]pyrazin-3(7H)-1 hydrochloride (MCLA) chemiluminescence assay using FluoSTAR OPTIMA, BMG labtech. For NOX2, a semi-recombinant system was used as previously described with the modification that MCLA (10 µM) was used instead of L-012 (Diebold and Bokoch, 2001). For NOX5, 4 µg of membrane protein was prepared in a final volume of 150 µL per well in the presence of HEPES (50 mM, pH 7.5), NTA (0.3 mM), HEDTA (0.3 mM), 1,2-bis(2-aminophenoxy)ethane-N,N,N',N'-tetraacetic acid (BAPTA) (0.3 mM), flavin adenine dinucleotide (10 µM), MgCl₂ (1 mM), phosphatidic acid (1,2 didecanoyl-sn-glycerol-3-phosphate, Sigma) (5.5 µM), MCLA (10 µM), CaCl₂ (700 µM) and various concentrations of inhibitors were added. Reactions were performed at 37°C and initiated by adding NADPH (200 µM). Superoxide generation was determined by measuring the MCLA light emission every 0.5 s in a luminometer for 120 cycles at 37°C, and determining the peak.

The generation of superoxide by the xanthine/xanthine oxidase was performed in PBS supplemented with xanthine oxidase (0.1 U·mL⁻¹), EDTA (0.3 mM), MCLA (0.1 mM). The reaction was started by the addition of xanthine (0.5 mM). Superoxide dismutase (SOD)-inhibitable luminescence of each well was measured for 0.5 s in a luminometer for 60 cycles at 37°C.

Oxygen consumption

The effect of inhibitors on the consumption of oxygen by stimulated neutrophils was assessed using a Clark-type electrode (oximeter). The electrode was prewarmed to 37°C, and bathed in saturated KCl. It was then allowed to stabilize in HBSS for approximately 15 min. For each recording, 1 × 10⁶–1 × 10⁷ cells were used. Cells were prewarmed (with inhibitors where indicated) for 15 min at 37°C. Cells were then placed into the oximeter and recorded for 5 min. Where indicated, cells were then stimulated with PMA (2 µM) or ionomycin (2 µM) and recorded for 20 min. The oxygen content of air-saturated buffer was taken to be 240 nmol·mL⁻¹. Viability of neutrophils was assessed using calcein, as described below.

Cell viability

Cell viability was assessed using calcein and the alamarBlue® assay (Invitrogen) using FluoSTAR OPTIMA, BMG labtech. Fluorescence was recorded with 485 nm excitation and 520 nm emission wavelengths for calcein and 550 nm excitation and 590 nm emission wavelengths for alamarBlue®. Cells were washed with HBSS to remove medium and resus-

pended in HBSS at 500 000 cells·mL⁻¹. Cells were seeded into 96-well plates at a density of 50 000 cells (100 µL). In addition, a standard curve of a known number of viable cells was included on the plate. For neutrophils used for the oximeter study 10⁶–10⁷ cells·mL⁻¹ were used. Cells were pre-incubated with the indicated concentration of inhibitor for 10 min in the dark at room temperature. Calcein (2 µL) was then added to a final concentration 4 µM while 10 µL alamarBlue® solution was added. Cells were incubated at 37°C in the dark for 30 min before being measured. The number of viable cells was determined by comparison to the standard curve.

p47^{phox} translocation

To examine the effect of celastrol on the assembly of the NADPH oxidase, isolated neutrophils were prepared as previously described. Neutrophils were resuspended (PBS with added Ca²⁺ and magnesium) and suspensions (5 × 10⁶ mL⁻¹) were exposed to DMSO (0.05%) (carrier control), staurosporine (200 nM), celastrol (1 and 5 µM) for 10 min at room temperature with occasional mixing. Neutrophils were then challenged with buffer or PMA (100 ng·mL⁻¹) for 10 min at 37°C with tumbling. Neutrophils were pelleted, disrupted by sonication and membranes isolated as done previously (Clark *et al.*, 1990) and translocation of p47^{phox} in stimulated neutrophils was assessed as previously reported using rabbit polyclonal antibody against p47^{phox} (1:20 000 dilution) followed by donkey anti-rabbit HRP (Amersham; dilution 1:50 000) (Clark *et al.*, 1990). Membrane-associated p47^{phox} was quantified using a phosphorimager.

Tandem SH3 p47^{phox} competitive pull-down assay

The regions corresponding to the tandem SH3 domains of p47^{phox} (residues 156–285) and NOXO1 (residues 157–290) were amplified by PCR using cDNA extracted from human neutrophils and colon, respectively, and were cloned into the expression vector pGEX-6P-1. The generated plasmids were transformed into BL-21 bacteria. Protein expression was induced by 3 h incubation with 1 mM isopropyl-1-thio-β-d-galactopyranoside (IPTG) at 37°C and glutathione-S-transferase (GST) fusion proteins were purified according to the manufacturer's protocol. Briefly, the bacterial pellet was harvested, lysed by sonication in lysis buffer Tris (50 mM, pH 7.0), NaCl (300 mM), EDTA (2 mM), DTT (4 mM) and protease inhibitors (Roche); The lysate was centrifuged for 10 min at 4°C, 12 000 × g. The soluble fraction was incubated for 1 h at 4°C with glutathione-sepharose beads (Amersham Bioscience) and washed successively with 50 mL of washing buffer I [Tris (50 mM, pH 7.0), NaCl (1 M), EDTA (2 mM), DTT (4 mM) and 100 mL of washing buffer II consisting of Tris (50 mM, pH 7.0), NaCl (50 mM), EDTA (2 mM), and DTT (4 mM)]. Purity was evaluated by SDS-PAGE and Coomassie Blue staining. GST fusion proteins attached to the beads were used directly for the competitive pull-down assay.

GST-(SH3)₂ proteins bound on glutathione sepharose (1.5 µM) were combined in a final volume of 300 µL with a peptide corresponding to the proline rich region of p22^{phox} (QPPSNPPPRPP at 1.5 µM) fluorescently labelled at the N-terminus with 5-FAM (Molecular probes) and incubated for 45 min at RT with slight agitation. Following incubation, the

complex formed by the beads, GST-(SH3)₂ proteins and the fluorescent peptide was recovered by centrifugation for 5 min, RT at 6082 × g in a microcentrifuge. After removal of the supernatant, the beads were washed 3 times in 500 µL washing buffer II. Finally, the bound fluorescent peptide was resuspended in 200 µL washing buffer II and fluorescence was measured (at λ485 nm for the excitation filter and λ520 nm for the emission filter using FluoSTAR OPTIMA, BMG labtech). For competition studies, unlabelled p22^{phox} peptide, unlabelled p22^{phox} mutated peptide (R158-A), celastrol and DPI were added to the mixture. To verify that equal amounts of GST-(SH3)₂ proteins were present in the beads after the pull-down experiments, SDS-PAGE was performed followed by Coomassie blue staining.

Fluorescence measurements

Recombinant p47^{phox} protein used for fluorescence measurements and native mass spectrometry has been produced and purified as previously described (Durand *et al.*, 2006). All experiments were performed at 25°C in a quartz cuvette containing a stir bar, using a Photon Technology International Quanta Master I spectrofluorometer. The measurements were automatically corrected for intensity fluctuation in lamp emission. All spectra were corrected for buffer fluorescence. Fluorescence measurements were routinely carried out after dilution of recombinant p47^{phox} (140 nM final concentration) and equilibration for 30 min in 1 mL of buffer containing 50 mM HEPES, pH 7.5, 500 mM NaCl, 1 mM EDTA, 2 mM dithiothreitol (DTT) and 10% glycerol. Celastrol was then added and the emission fluorescence was scanned in the range of 310–380 nm (4 nm bandwidth), upon excitation at 295 nm (2 nm bandwidth). Binding of celastrol with time (0 min to 20 min), was monitored by the variation of tryptophan-intrinsic fluorescence of p47^{phox} (between 310 nm and 380 nm) produced after addition of celastrol.

Native mass spectrometry characterization

Non-covalent mass spectrometry measurements were performed by using a Q-TOF Micro mass spectrometer (Waters, Manchester, UK) equipped with an electrospray ion source. It operated with a needle voltage of 2.8 kV, sample cone and extraction cone voltages, respectively, of 80 V and 5 V; backing Pirani pressure was set at 7 mbar. Recombinant p47^{phox} (1-342) was extensively dialysed against 500 mM ammonium acetate pH 7.5. Myoglobin from horse skeletal muscle was purchased from Sigma Aldrich and directly dissolved in 500 mM ammonium acetate pH 7.5. Protein was diluted 10 times in water to reach a final concentration of 16 µM just before injection. Celastrol (4.44 mM) dissolved in DMSO/EtOH (1:4 v:v), or DMSO/EtOH (1:4 v:v) was added to the protein solution before infusion at a flow rate of 20 µL·min⁻¹. The mass spectra were recorded in the 1000–5000 mass-to-charge (m/z) range. Data were acquired in the positive mode and calibration was performed using the multiply charged states produced by a separate injection of heart horse myoglobin dissolved at 300 nM in water/acetonitrile (1:1 v:v) with 0.2% formic acid. Data were processed with MassLynx 4.0 (Micromass) and deconvoluted with Magtran software (Zhang and Marshall, 1998).

Statistics

For the inhibition of ROS generation as detected by Amplex Red, Graph-Pad Prism software was used to fit sigmoidal dose–response curves, from which EC_{50} values and Hill slopes were obtained.

For clarity, toxicity data are presented as % control, however the viable cell numbers were used for statistical analysis in a two-way ANOVA, and where warranted, this was followed by Dunnett's *post hoc* analysis for repeated measures. The latter analysis avoids using a control with zero variance (Lew, 2007). In some instances, the toxicity at 1 μ M and 10 μ M was interpolated (Microsoft, Excel) from serial dilution curves, which began at 100 μ M, and therefore fell at 12.5 μ M and 1.56 μ M.

For clarity, oximeter data are presented as % control; however, the rate of oxygen consumption ($\text{nmol}\cdot\text{min}^{-1}$ per 10^7 cells) was used for statistical analysis in a one-way ANOVA for repeated measures with Bonferroni's multiple comparison test *post hoc* analysis (Graph-Pad, Prism).

Chemicals and reagents

DMEM, RPMI 1640 with glutamax, HBSS, FBS, 5-carboxyfluorescein (5-FAM), 2-methyl-6-(4-methoxyphenyl)-3,7-dihydroimidazol[1,2-a]pyrazin-3-one (MCLA) and Amplex Red were purchased from Invitrogen. Penicillin, streptomycin, PMA, apocynin, calcein, DPI chloride, DTT, IPTG, SOD, trolox, xanthine, xanthine oxidase were purchased from Sigma Aldrich, Celastrol was purchased from Cayman Chemical (Ann Arbor, MI, USA), Ficoll-Paque™ PLUS and glutathione sepharose beads high performance were purchased from Amersham Biosciences (Uppsala, Sweden).

Results

Celastrol inhibits hydrogen peroxide release by human NOX1, NOX2, NOX4 and NOX5 in intact cells

To test the effect of celastrol on NOX NADPH oxidase activity, ROS generation was determined in four cell lines: (i) induced PLB-985 cells that, upon differentiation into a neutrophil-like phenotype, express NOX2 and produce ROS in response to PMA (0.1 μ M); (ii) a CHO cell line expressing human p22^{phox}, NOXO1, NOXA1 and NOX1 that also produces ROS upon addition of PMA (0.1 μ M); (iii) an HEK293T NOX4 inducible cell line that, upon addition of tetracycline, expresses NOX4 and produces ROS spontaneously (Serrander *et al.*, 2007a); and (iv) an HEK cell line stably expressing NOX5 that produces ROS in response to Ca^{2+} influx induced by the ionophore ionomycin (1 μ M) (Serrander *et al.*, 2007b). Hydrogen peroxide production was measured as the conversion of Amplex Red into the fluorescent product resorufin. Following 10 min pre-incubation, both celastrol and DPI potently and effectively inhibited the four NOX isoforms tested (Figure 1) with an IC_{50} in the low micromolar range (Table 1). The profile for the inhibition by DPI was similar among all NOX enzymes tested with IC_{50} s that ranged 20–240 nM and a similar shape of the dose–response curve for all four isoforms. In contrast, celastrol demonstrated selective inhibition of

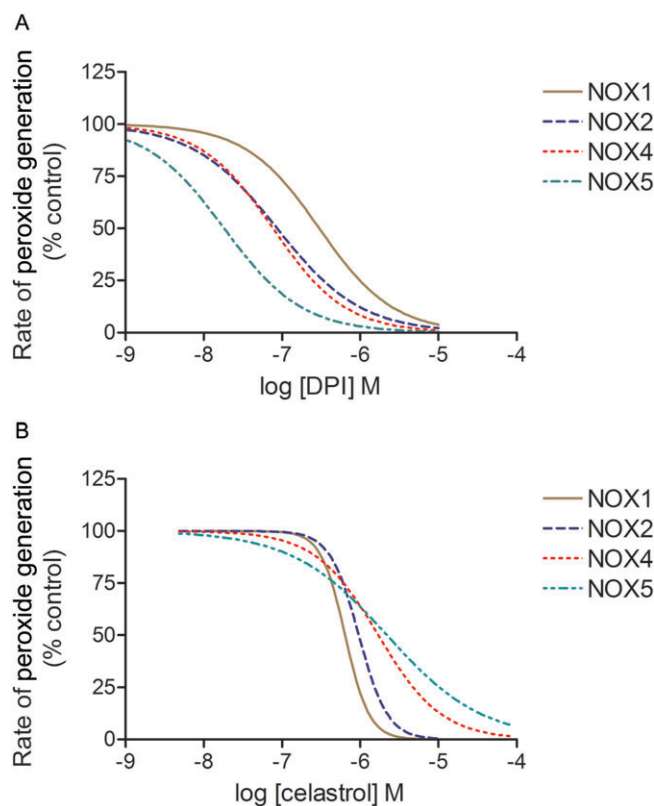


Figure 1

Celastrol and DPI inhibit hydrogen peroxide production in whole cells. Representative concentration–response curves for the inhibition of NOX1, NOX2, NOX4 and NOX5 by celastrol (A) and DPI (B). Cells were pre-incubated for 15 min with celastrol, then stimulated by PMA (0.1 μ M) for CHO-NOX1 and PLB-985 (NOX2), or ionomycin (1 μ M) for HEK-NOX5. For HEK-NOX4, tetracycline (1 $\mu\text{g}\cdot\text{mL}^{-1}$) was added 18 h before measurement. The rate of reactive oxygen species generation was determined as the change in fluorescence over a 10 min period beginning 10 min after stimulation (or 25 min after addition of celastrol in the case of NOX4). Data were normalized to control response in each case and fitted using a sigmoidal dose–response curve (Graph-Pad).

NOX isoforms. Inhibition of NOX1 and NOX2 was more efficient, with IC_{50} s of 410 and 590 nM, respectively, in comparison to 2.7 and 3.13 μ M for NOX4 and NOX5, respectively. The inhibition curve was significantly steeper for NOX1 and NOX2, with Hill slopes of 2.18 and 2.07, respectively, whereas those for NOX4 and NOX5, had Hill slopes closer to 1 (1.11 and 0.92 respectively) (Table 1). The steeper Hill slopes suggest positive co-operativity in the inhibition of NOX1 and NOX2 by celastrol.

Inhibition of ROS generation by celastrol is due neither to toxicity nor to a ROS scavenging effect

To determine if the observed inhibitory effect of celastrol on NOX activity was a consequence of cytotoxicity, we examined cell viability in two ways using the intracellular fluorescent probe calcein which is cleaved by esterases and retained

Table 1

Summary of the values of IC₅₀s and Hill slopes for celastrol and diphenyleneiodonium (DPI) for NOX1, NOX2, NOX4 and NOX5 expressing cells

	NOX1		NOX2		NOX4		NOX5	
	IC ₅₀ (μM)	Hill						
Celastrol	0.41 ± 0.20	2.18 ± 0.69	0.59 ± 0.34	2.07 ± 0.43	2.79 ± 0.79	1.18 ± 0.15	3.13 ± 0.85	0.92 ± 0.53
DPI	0.24 ± 0.08	0.83 ± 0.11	0.10 ± 0.03	0.80 ± 0.24	0.09 ± 0.02	0.85 ± 0.15	0.02 ± 0.01	1.35 ± 0.47

Data are presented as mean ± SD of 3–8 values.

inside live cells and using the fluorescent probe Alamar Blue, which is reduced to a fluorescent product in metabolically active cells. Both calcein and Alamar Blue staining indicated that celastrol was toxic to PLB-985 at 10 μM (Figure 2A). Results from calcein studies also indicated 10 μM had some toxicity to HEK cells. Importantly, the inhibition of NOX activity by celastrol occurred at concentrations where no cytotoxicity was observed. Alamar Blue reduction was inhibited by DPI in the HEK and PLB cell lines; however, as this reduction is dependent on mitochondrial flavoproteins, this may in part represent enzyme inhibition by the flavoprotein inhibitor DPI, and not necessarily cellular toxicity. The calcein results indicate that DPI was not toxic on any of the cell lines at 10 μM.

The possibility that celastrol was reducing the amount of detectable hydrogen peroxide by scavenging the precursor, superoxide, was assessed using the superoxide-generating enzymatic system xanthine/xanthine oxidase (Figure 2B). In contrast to the actions of DPI, which directly inhibits xanthine oxidase, SOD, which dismutates superoxide into hydrogen peroxide, and trolox, which is a potent radical scavenger, celastrol did not show a concentration-dependent inhibition of MCLA-induced luminescence. Similarly, levels of hydrogen peroxide detected by Amplex Red were not significantly diminished by celastrol, whereas they were significantly decreased both by DPI, and by the hydrogen peroxide metabolizing enzyme catalase. Taken together, these data exclude scavenging ROS and interference with ROS detection assays as explanations for the observed reduction of oxidant detection by NOX enzymes in the presence of celastrol.

Celastrol inhibits NOX enzyme activity but not translocation of p47^{phox}

When active, NOX enzymes catalyse the reduction of oxygen to superoxide, which subsequently dismutates into hydrogen peroxide, either spontaneously or catalysed by SOD. As there was no evidence for oxidant scavenging by celastrol, we aimed to determine if celastrol was a *bona fide* inhibitor of NOX enzymes, in which case it should block consumption of oxygen, the substrate of NOX-catalysed reduction. Stimulated human neutrophils were used to assess NOX2 activity because they express high levels of NOX2 and generate very large amounts of ROS from molecular oxygen. The basal level of oxygen consumption by unstimulated neutrophils was measured during the first 5 min and was followed by stimulation with PMA. Stimulated neutrophils consumed oxygen at a rate of 22.5 nmol·min⁻¹ per 10⁷ cells that was completely

blocked by either celastrol (10 μM) or DPI (10 μM) (NOX2 panel) without affecting cell viability, as determined by calcein under these conditions (data not shown). As expected and in contrast to DPI or celastrol, the potent oxidant scavenger trolox (1 mM) had no effect on oxygen consumption but significantly reduced the level of hydrogen peroxide generated by stimulated neutrophils (Figure 3B). Cells expressing NOX1, NOX4 or NOX5 were less robust in their oxygen consumption. For these cells, celastrol did not completely block oxygen consumption. DPI on the other hand, which blocks NOX enzymes as well as mitochondrial respiration at this concentration, completely blocked oxygen consumption in these cells. Nevertheless, both celastrol and DPI inhibited the additional consumption of oxygen introduced by the addition of these NOX isoforms to the cells.

Because the Hill slopes for inhibition of NOX1 and NOX2 were suggestive of a positive co-operative interaction of celastrol with these cytosolic subunit-dependent NOX isoforms, we postulated that celastrol may have an effect on the cytosolic subunits. To investigate whether celastrol interfered with the PKC-dependent translocation of the cytosolic factor p47^{phox}, human neutrophils were incubated with celastrol, then stimulated with PMA and homogenized to isolate the membrane fractions. Immunoblots of membranes using a specific p47^{phox} antibody showed that p47^{phox} translocation was not inhibited by celastrol (1 and 5 μM), whereas it was inhibited by staurosporine (200 nM), an inhibitor of PKC (Figure 3C) previously demonstrated to block phosphorylation-dependent translocation of p47^{phox} (Nauseef *et al.*, 1991), a prerequisite for oxidase assembly and activity (Heyworth *et al.*, 1991). These data demonstrate that celastrol did not inhibit PKC and did not block the translocation or the binding of p47^{phox} to the stimulated neutrophil membrane.

Celastrol inhibits superoxide production by NOX2 and NOX5 in cell-free assays

In order to test a direct inhibitory effect of celastrol on NOX enzymes, cell membranes were prepared from human neutrophils and from NOX5 expressing-HEK cells. NOX2-containing neutrophil membranes were incubated in the presence of recombinant cytosolic factors, whereas NOX5-containing membranes were incubated in the presence of an elevated concentration of Ca²⁺ (700 μM). The reaction was initiated by addition of NADPH, and superoxide production was immediately measured as MCLA luminescence. Both DPI and celastrol caused a concentration-dependent inhibition of NOX2 and NOX5 activities (Figure 4), with DPI exhibiting

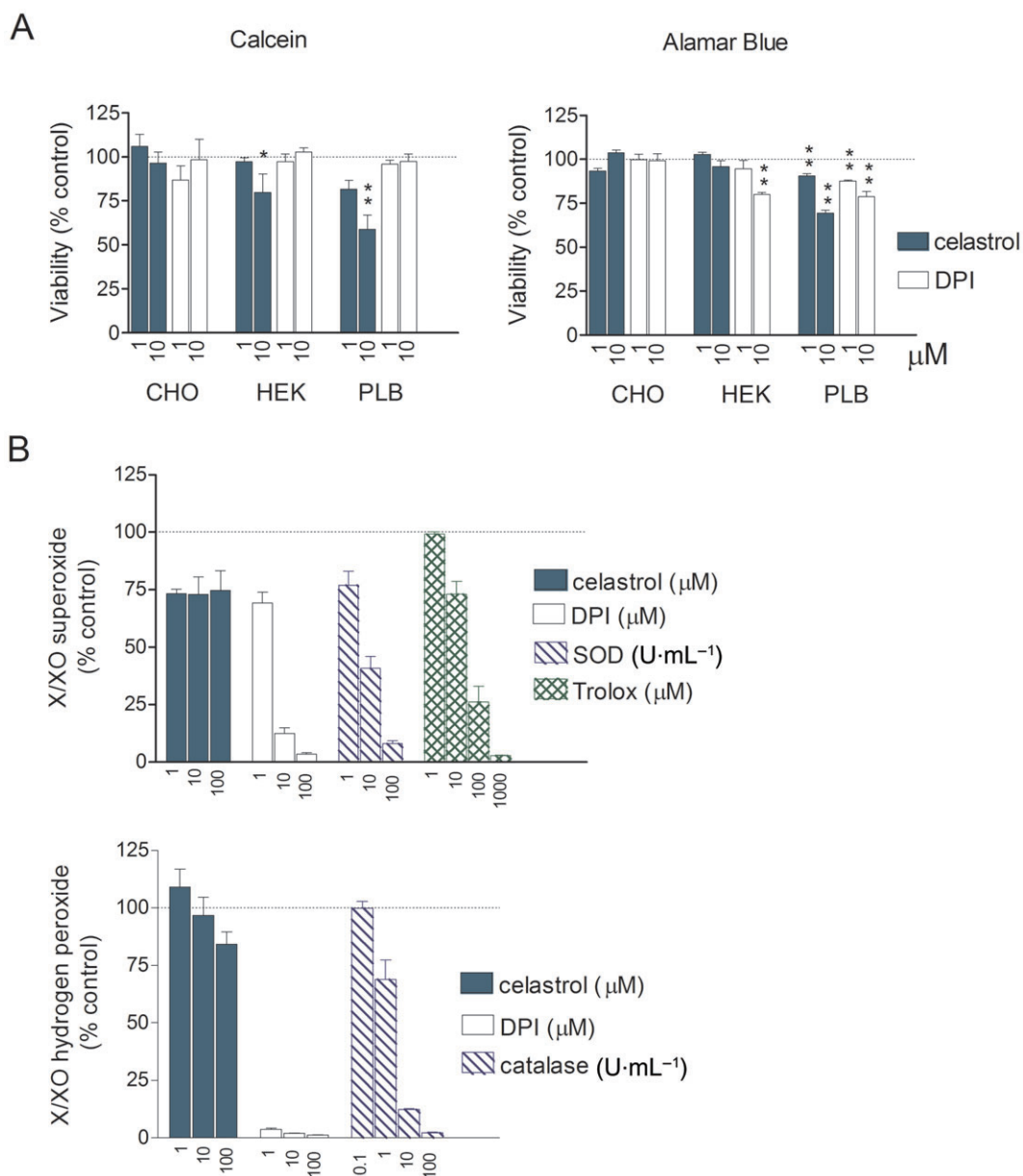


Figure 2

Inhibitory action of celastrol on NOX enzymes is not due to cellular toxicity or scavenging of reactive oxygen species. (A) Toxicity: Bars represent the percent viable CHO, HEK or PLB-985 cells following 30 min treatment with 1 μM or 10 μM celastrol or DPI, as determined by calcein (left) or Alamar Blue (right). Columns represent the mean and SEM of three to seven experiments. Asterisks indicate a significant difference from control as determined by repeated measures ANOVA followed by Dunnett's *post hoc* analysis (** $P < 0.01$). (B) Superoxide and hydrogen peroxide generation by the xanthine/xanthine oxidase superoxide generating system: The amount of superoxide detected using the superoxide specific probe MCLA (upper) or hydrogen peroxide measured using the probe Amplex Red (bottom) in the presence of several concentrations of celastrol, DPI, SOD or catalase or trolox, was measured. A concentration-dependent decrease of the MCLA luminescent signal was observed with the superoxide scavengers SOD and trolox and with DPI, which is known to inhibit xanthine oxidase. As anticipated, a concentration-dependent decrease of the Amplex Red signal was observed with catalase. Superoxide is expressed as a % of the control value, and columns represent the mean and SEM of three independent experiments.

very similar IC_{50} and Hill slopes for both NOX2 and NOX5 (Table 2). In contrast to the effect of DPI on the NOX isozymes in the cell-free system but similar to what was observed in the cellular assays, celastrol was a more potent inhibitor of the NOX2 system, with an IC_{50} of 1.24 μM versus 8.3 μM for NOX5 (Table 2). In addition, whereas the Hill

slope for celastrol was ~ 1 for NOX5, it was closer to 2 for NOX2 in both the cell-free and whole-cell assays. Unlike DPI or celastrol, triptolide, a major constituent of *Tripterigium wilfordii* extracts, did not block superoxide generation by either NOX2 or NOX5, even at higher concentrations (100 μM) (Figure 4).

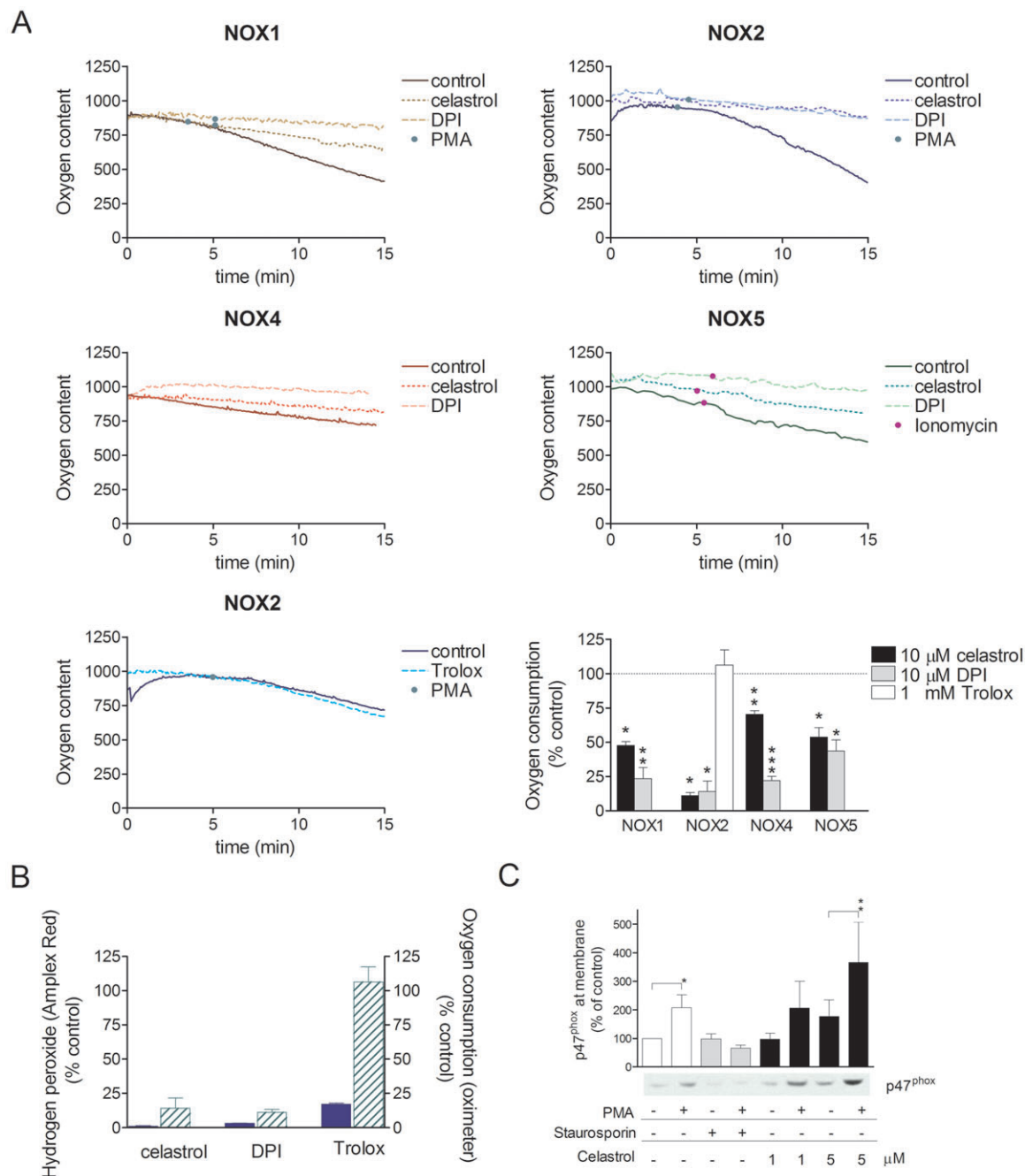


Figure 3

Celastrol and DPI inhibit NOX activity. (A) Celastrol and DPI block oxygen consumption in whole cells: Representative curves of oxygen consumption for CHO-NOX1, neutrophils, HEK-NOX4 and HEK-NOX5. Cells were pre-incubated for 15 min alone or with 10 μ M of celastrol or DPI. Measurements were taken in whole cells following stimulation with 0.1 μ M PMA (NOX1 and neutrophils), or with 1 μ M ionomycin (NOX5). For HEK-NOX4, tetracycline (1 μ g·mL⁻¹) was added 18 h before measurement. The columns in the histogram represent the mean and SEM for the oxygen consumption following celastrol, DPI or Trolox, expressed as % of control. (B) Celastrol and DPI block oxygen consumption but are not ROS scavengers. The columns on the left of each pair (solid blue) represent the hydrogen peroxide measured by Amplex Red while the right hand columns (green hatched) represent the oxygen consumption measured by the oximeter for celastrol (10 μ M), DPI (10 μ M) and Trolox (1 mM). Data are expressed as % control. Columns are the mean \pm SD, $n = 3$. Asterisks indicate a significant difference from control as determined by a repeated measures ANOVA followed by Bonferroni's *post hoc* analysis performed on the rate of consumption data prior to normalization ($*P < 0.05$, $**P < 0.001$, $***P < 0.0001$). (C) Celastrol does not inhibit translocation of p47^{phox} to the membrane: columns represent the relative change in the density of the p47^{phox} on an immunoblot of membranes from cells that had been treated with PMA compared with cells without PMA stimulation. The p47^{phox} translocation was inhibited by pretreatment with 200 nM of the PKC inhibitor staurosporine, but celastrol 1 μ M and 5 μ M had no effect on the translocation of p47^{phox}. The means and SEM of five experiments are shown. A representative immunostained blot is shown below the graph.

Table 2

Summary of the values of IC₅₀s and Hill slopes for celastrol and diphenyleneiodonium (DPI) for NOX1, and NOX2 particulate assays

	NOX2 IC ₅₀ (μM)	Hill	NOX5 IC ₅₀ (μM)	Hill
Celastrol	1.24 ± 0.60	1.68 ± 0.16	8.40 ± 3.80	1.03 ± 0.05
DPI	0.08 ± 0.02	1.16 ± 0.11	0.04 ± 0.02	0.94 ± 0.19

Data are presented as mean ± SD of 3–8 values.

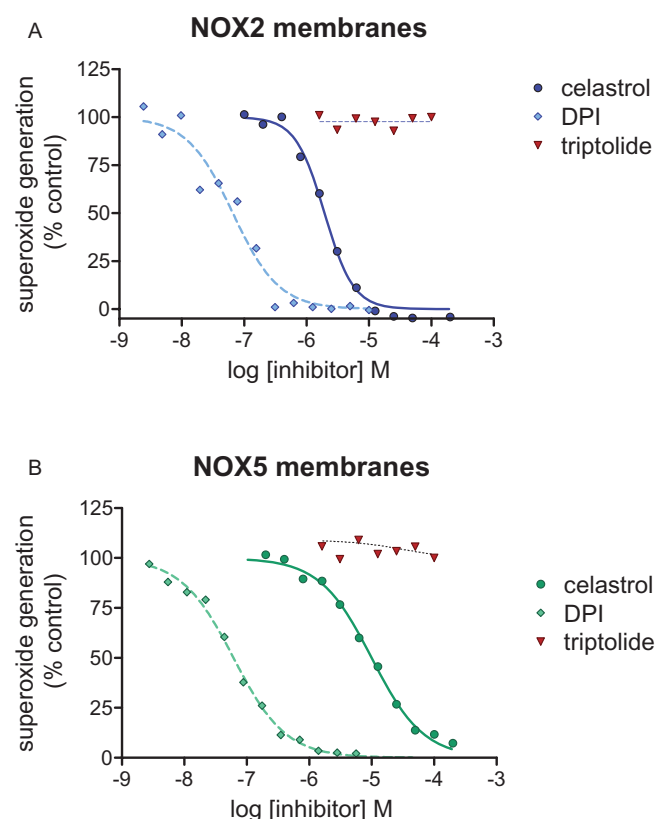


Figure 4

Celastrol and DPI inhibit superoxide generation by particulate membrane fractions. Representative concentration–response curves for the inhibition of NOX2 and NOX5. Celastrol and DPI, but not triptolide inhibited superoxide generation in the NOX2 semi-recombinant reconstituted system comprising purified neutrophil membranes and recombinant rac GTPase and p47-p67 chimeric protein (A) and in the NOX5 system comprising purified membranes of HEK cells overexpressing NOX5 in controlled high Ca²⁺ (700 μM) concentration (B). The reaction was initiated by the addition of NADPH and MCLA enhanced luminescence was measured for one minute to determine the peak luminescence. Data were normalized to control response in each case and fitted using a sigmoidal dose–response curve (Graph-Pad).

Celastrol disrupts the binding of p22^{phox} and the tandem SH3 domain of p47^{phox} and NOXO1

In order to examine in more depth the mechanisms by which celastrol inhibited cytosolic subunit-dependent NOX1 and

NOX2, we used an *in vitro* pull-down assay to determine if celastrol inhibited the binding of the cytosolic NOX organizers NOXO1 and p47^{phox} to the membrane target protein p22^{phox}. GST fusion recombinant proteins encompassing the SH3 domains of NOX organizers NOXO1 and p47^{phox} were incubated with a fluorescently-labelled peptide containing a proline-rich region of p22^{phox} in the presence of DPI or celastrol. Following recovery of complexes by centrifugation and washing, fluorescence was measured. For both NOXO1 and p47^{phox}, the presence of excess celastrol decreased the amount of the bound fluorescent peptide in a concentration-dependent fashion, whereas DPI had no effect on the binding-dependent fluorescence (Figure 5). This inhibition by celastrol was not due to the GST-fusion protein being released from the beads, but rather to the fluorescent peptide being displaced from the binding pocket, as equal amounts of the GST fusion protein could be detected in the pellet by SDS-PAGE (data not shown). The binding of GST-p47^{phox} and GST-NOXO1 to the p22^{phox} peptide was specific, as five to ten times excess of unlabelled p22^{phox} peptide competitively prevented the binding of the fluorescent peptide. In contrast, a peptide containing a substitution for a residue crucial for the p22^{phox} binding (Arg158-Ala) (Nobuhisa *et al.*, 2006; Yamamoto *et al.*, 2007) had no effect on binding. These data demonstrate that the binding of celastrol to sites in p47^{phox} or NOXO1 compromises interaction of these cytosolic NOX subunits to the membrane target in p22^{phox}.

Specific binding of celastrol to p47^{phox}

We tested whether celastrol interacted with recombinant p47^{phox} (1-342), using both intrinsic fluorescence (Figure 6A) and native mass spectrometry (Figure 6B) for analysis, because celastrol showed an apparent co-operative inhibition of NOX1 and NOX2, which require cytosolic subunits for function, and not of NOX4 and NOX5, which are either constitutively active or depend on Ca²⁺ activation, and because celastrol disrupted the interaction between tandem SH3 domain of p47^{phox} or NOXO1 and the proline rich region of p22^{phox} in the GST-pull down assay.

Intrinsic tryptophan fluorescence is commonly used to monitor protein conformational changes (Swain *et al.*, 1997) or ligand binding (Jault *et al.*, 2000). Celastrol quenched p47^{phox} fluorescence, reflecting an interaction between the ligand and the protein (Figure 6A, upper right). Quenching was effective after 2.5 min and increased over 20 min, probably due to the progressive celastrol binding to p47^{phox}. We were not able to measure quenching before 2.5 min and after 20 min because of issues related to signal stability. Because the celastrol stock solution contained 100% DMSO and the

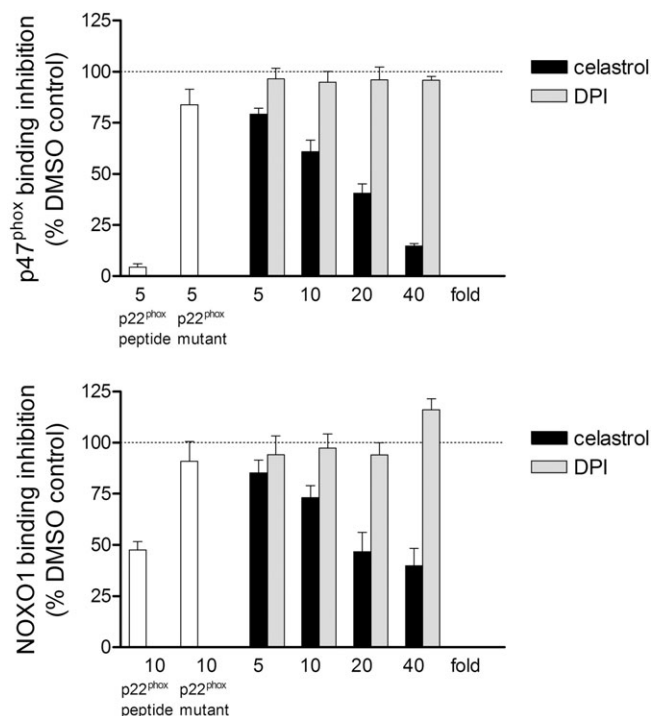


Figure 5

Celastrol inhibits the binding of a p22^{phox} proline-rich peptide to its ligand, the tandem SH3 domain of p47^{phox}. The amount of binding between the proline-rich region of p22^{phox} and the SH3 domain of the NOX organizer proteins p47^{phox} (top) or NOXO1 (bottom) in the presence of celastrol or DPI was determined. Glutathione beads attached to recombinant GST-SH3 domains from p47^{phox} and NOXO1 were incubated in the presence of a fluorescently labelled p22^{phox} peptide. After 45 min, the complex was pulled down and fluorescence was measured. Competition with an unlabelled p22^{phox} peptide disrupted the binding, whereas neither DPI nor a mutated p22^{phox} peptide failed to disrupt the binding. Data were normalized to control response in each case. Columns represent the mean and SEM of three independent experiments.

final concentration of DMSO in the reactions was 1.2%, we assessed the effects of DMSO directly on fluorescence and found no effect (Figure 6A, upper left). N-acetyltryptophanamide (NATA) was used to exclude an inner-filter effect of celastrol under the same conditions (data not shown).

In order to confirm that celastrol interacted directly with p47^{phox}, we employed mass spectrometry to detect complexes under native conditions. Deconvoluted spectra obtained for p47^{phox} (1-342) (MW = 40399.0 Da) (Figure 6B) after incubation with celastrol revealed the presence of three adducts at +450 Da, +901 Da and +1351 Da, corresponding to the mass of one, two or three molecules of celastrol (MW = 450.6 Da). Binding occurred after incubation with p47^{phox}: celastrol molar ratio of 1:3 (data not shown) and increased in a concentration-dependent manner (Figure 6B; compare without or with a 1:9 molar ratio). Binding specificity is further confirmed by the absence of adducts observed when incubating horse myoglobin with celastrol under similar conditions (Figure 6C). The additional peaks in the spectra

acquired for myoglobin corresponded to sodium adducts (+22 Da). A similar lack of celastrol binding was observed for lysozyme (data not shown). Collectively, data from both intrinsic fluorescence quenching and mass spectrometry suggest that celastrol interacted specifically with p47^{phox}.

Discussion

The central role of NOX enzymes in a wide-range of important biological processes provides a powerful incentive to identify specific, effective and nontoxic inhibitors. Although a number of molecules have been demonstrated to inhibit NOX enzymes, very few compounds were evaluated comprehensively, and most studies focused their attention primarily on NOX2 (Jaquet *et al.*, 2009). In spite of numerous side effects (Aldieri *et al.*, 2008), DPI and apocynin remain the standards with which NOX inhibitors will be compared. The present study demonstrates that the natural compound celastrol is an effective and genuine inhibitor of NADPH oxidases. Analysing the effects of celastrol on different NOX isoforms in intact cells and broken cell reconstitution assay, we found direct effects of celastrol on enzyme activity and excluded cell toxicity or oxidant-scavenging as contributing to the observed inhibition. We systematically compared the inhibitory activity of celastrol with that of DPI, a potent flavoprotein inhibitor, the oxidant scavengers trolox, catalase, and SOD, and triptolide, another major component of *Trypterygium wilfordii*.

Celastrol completely inhibited the production of ROS by four NOX isoforms, including those that are dependent on cytoplasmic subunits (NOX1 and NOX2) and those that function independently of cytoplasmic subunits, including the constitutively active (NOX4), and calcium-dependent (NOX5) isoforms. The IC₅₀ and the shape of the dose-response curves for the inhibition of the individual NOX isoforms by celastrol exhibited important differences. Celastrol produced both larger Hill slopes and lower IC₅₀ for inhibition of NOX1 and NOX2 compared with NOX4 and NOX5, in experimental systems utilizing intact cells and membranes and in using two different ROS detection systems (Amplex Red and MCLA). The difference in the inhibition profile for the NOX isoforms may reflect the fact that NOX1 and NOX2 are subunit-dependent. The Hill slopes for NOX4 and NOX5 were close to 1, the value expected when a single drug molecule interacts with a single target to produce an effect (O'Donnell *et al.*, 1993), as is the case for DPI. The celastrol inhibition curves for NOX1 and NOX2 on the other hand had steeper Hill slopes, which can indicate the presence of co-operative binding, whereby a molecule possesses several binding sites that together inhibit a target enzyme. Furthermore, celastrol blocked the activity of the assembled NOX2 oxidase, as agonist-dependent phosphorylation and translocation of p47^{phox} was unaffected by treatment of intact neutrophils with celastrol. Consistent with this hypothesis, celastrol bound specifically to a recombinant p47^{phox} protein and interfered with interactions between the tandem SH3 domain of p47^{phox} and NOXO1 and the proline rich region of p22^{phox}. Whereas immunoblotting demonstrated that celastrol did not prevent p47^{phox} translocation to the plasma membrane, the pull-down assay showed that celastrol displaced

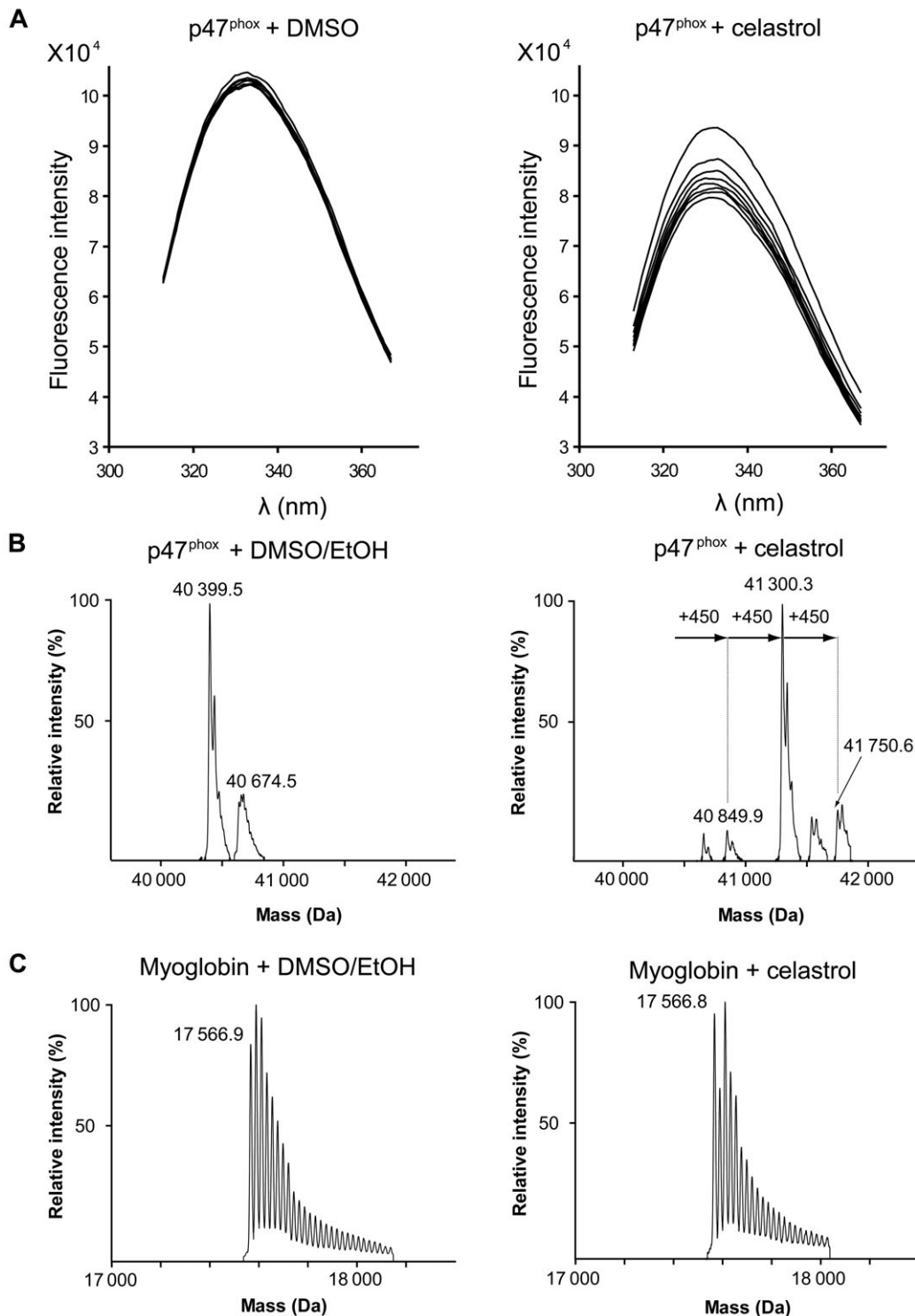


Figure 6

(A) Celastrol quenches p47^{phox} fluorescence. Recombinant p47^{phox} (1-342) was treated with celastrol (molar ratio 1:9) and the binding over time was analysed in a scanning fluorimeter using an excitation wavelength of 295 nm. The background signal from buffer alone was subtracted from the spectra shown. The spectra shown from top to bottom represent p47^{phox} treated with 1.2% DMSO (left) and celastrol (right), after 0, 2.5, 7.5, 10, 12.5, 15, 17.5 and 20 min. (B) Celastrol molecules bind p47^{phox}. Deconvoluted noncovalent mass spectrum of p47^{phox} with DMSO or p47^{phox} with celastrol (molar ratios 1:9). Peak at 40 400 Da corresponds to the celastrol-free protein, whereas peaks at 40 850 Da, 41 301 Da and 41 751 Da match the mass of one, two and three adducts of celastrol (450.6 Da), respectively. (C) Celastrol molecules do not bind myoglobin: Deconvoluted noncovalent mass spectrum of horse myoglobin with DMSO or myoglobin with celastrol (molar ratio of 1:9). Peaks at 17 566.8 Da and 14 305.5 Da correspond to the celastrol-free mass of myoglobin bound to its haem. The other peaks correspond to sodium adducts (+22 Da).

the p22^{phox} peptide from the tandem SH3 domain. Although the precise nature by which celastrol leads to this displacement remains unresolved, electrospray data show that celastrol bound to p47^{phox}, but no specific binding to the tandem SH3 domain was observed using either this technique or isothermal titration calorimetry (data not shown). It is thought that celastrol can react with the nucleophilic thiol groups of cysteine residues and form covalent Michael adducts (Salminen *et al.*, 2010). Thus, it is possible that celastrol can allosterically modify the protein p47^{phox}, as has been recently described for the disruption of the interaction between HSP90 and CDC37 (Zhang *et al.*, 2009). If confirmed experimentally, this would be a novel mechanism of action for inhibition of NOX proteins.

It is noteworthy that celastrol (10 μ M) incompletely inhibited oxygen consumption by NOX1-transduced CHO cells and NOX4- and NOX5-transduced HEK cells. The failure of celastrol to inhibit all oxygen consumption in these cells contrasts with the effect of DPI on the same cells and with the effect of celastrol on neutrophils, where inhibition is total. It is likely that mitochondria in the transfected cells are the source of celastrol-resistant but DPI-inhibited oxygen consumption, as DPI (10 μ M) inhibits mitochondrial ROS production (Li and Trush, 1998). In contrast to the behaviour of the transfected cells used, neutrophil production of oxidants is almost exclusively NOX2-dependant, as mitochondrial respiration in neutrophils is very low (Peachman *et al.*, 2001; Murphy *et al.*, 2003). Consequently, celastrol would be anticipated to be more effective in neutrophils than in cells with both mitochondrial and NOX enzymes consuming oxygen.

Our data demonstrate that celastrol inhibited the activity of all NOX isoforms tested, including both cytosolic factor-dependent and -independent species, and thus joins DPI and apocynin as a potential pharmacological tool to probe the activity and regulation of NOX enzymes. In the case of NOX2, the inhibitory effect of celastrol on p47^{phox} represents a novel mechanism: binding of celastrol to p47^{phox} and disruption of the association between p22^{phox} and the SH3 domains of p47^{phox} without compromising translocation of the cytosolic components in intact neutrophils. No previously described inhibitor blocks NADPH oxidase activity in this way, and definition of the precise mechanism whereby activity is decreased promises to provide important and novel insights into the adaptor function of p47^{phox}. In addition, celastrol must compromise other functional targets, as the cytosolic factor-independent NOX isoforms were also inhibited. DPI showed high potency (nanomolar range) for NOX, and XO, which are flavin-containing enzymes while celastrol was more specific for NOX as it did not inhibit XO.

Celastrol has a rather broad range of actions attributed to it, including inhibition of NF- κ B, ERK, TNF- α , IL-1, and NO (Allison *et al.*, 2001; Kim *et al.*, 2009), inhibition of heat-shock protein 90 (Zhang *et al.*, 2008), inhibition of the proteasome (Yang *et al.*, 2006) and inhibition of Kir2.1 and hERG potassium channels (Sun *et al.*, 2006). However, these effects occur following long exposure (hours) of cells or tissues to celastrol whereas the effects on NOX enzymes observed in the current study occurred within minutes. Although a direct effect of celastrol has been demonstrated in the case of heat shock protein 90, it is possible that some of the effects

observed hours following celastrol treatment derive, at least in part, from NOX inhibition.

Celastrol has been reported to decrease ROS generation by NOX1 in mouse microvascular endothelial cells (Wu *et al.*, 2009). In that study, celastrol (50–200 nM for 24 h) interfered with the induction of NOX1 expression in LPS- and IFN γ -treated endothelial cells, as shown by NOX1 immunostaining. In the present study, we demonstrated that celastrol rapidly and directly inhibits NOX1 activity.

In conclusion, celastrol exhibits several advantages over other agents and promises to be a useful analytical tool for use in isolated enzyme preparations or intact cells. Future studies are required to evaluate the usefulness of this agent as a specific and selective inhibitor of NOX enzymes in animal experimental systems. Certainly, the use of celastrol *in vivo* is feasible, as numerous studies have shown its efficacy in spite of its potential toxicity (reviewed in Salminen *et al.*, 2010). Inhibition of NOX enzymes has potential therapeutic potential in a wide variety of diseases including atherosclerosis, hypertension, stroke, Alzheimer's disease and amyotrophic lateral sclerosis among others. It is expected that such compounds will be tolerated as animals lacking NOX1, NOX2 or NOX4 are all viable, and rodents naturally lack the gene encoding NOX5. Whereas the total absence of NOX2 activity *in vivo* is associated with impaired immunity, carriers of this mutation with very low NOX2 expression are generally healthy (Kume and Dinauer, 2000) and patients who retain some residual production of ROS have a less severe disease (Kuhns *et al.*, 2010), suggesting that decreases in NOX2 activity do not necessarily lead to a complete loss of immune function. The characterization of celastrol as a NOX inhibitor adds an important tool for the study of the NADPH oxidase system, and also enhances our ability to interpret results of studies where this compound is employed.

Acknowledgements

The authors would like to thank Dr Pierre Maechler and Li Ning for their assistance with the oximeter studies, Hubert Gaertner and Paolo Botti for peptide synthesis, Jean-Michel Jault for advice regarding fluorescence experiments. Vincent Jaquet was supported by the Swiss innovation promotion agency CTI. Julien Marcoux was supported by a grant from the Association pour la Recherche contre le Cancer (ARC). The Nauseef lab is supported by NIH grant AI 70958 (WMN) and with resources and use of facilities at the Iowa City Department of Veterans Affairs (VA) Medical Center, Iowa City, IA 52246.

Conflicts of interest

Although K-H K, VJ and LF-C are founder members of Genkyotex SA, a start-up company developing NOX inhibitors, celastrol is not a compound developed by the company and therefore there are no conflicts of interest.

References

- Aldieri E, Riganti C, Polimeni M, Gazzano E, Lussiana C, Campia I *et al.* (2008). Classical inhibitors of NOX NAD(P)H oxidases are not specific. *Curr Drug Metab* 9: 686–696.
- Allison AC, Cacabelos R, Lombardi VR, Alvarez XA, Vigo C (2001). Celastrol, a potent antioxidant and anti-inflammatory drug, as a possible treatment for Alzheimer's disease. *Prog Neuropsychopharmacol Biol Psychiatry* 25: 1341–1357.
- Bedard K, Krause KH (2007). The NOX family of ROS-generating NADPH oxidases: physiology and pathophysiology. *Physiol Rev* 87: 245–313.
- Brinker AM, Ma J, Lipsky PE, Raskin I (2007). Medicinal chemistry and pharmacology of genus *Tripterygium* (Celastraceae). *Phytochemistry* 68: 732–766.
- Clark RA, Volpp BD, Leidal KG, Nauseef WM (1990). Two cytosolic components of the human neutrophil respiratory burst oxidase translocate to the plasma membrane during cell activation. *J Clin Invest* 85: 714–721.
- Cleren C, Calingasan NY, Chen J, Beal MF (2005). Celastrol protects against MPTP- and 3-nitropropionic acid-induced neurotoxicity. *J Neurochem* 94: 995–1004.
- Diebold BA, Bokoch GM (2001). Molecular basis for Rac2 regulation of phagocyte NADPH oxidase. *Nat Immunol* 2: 211–215.
- Durand D, Cannella D, Dubosclard V, Pebay-Peyroula E, Vachette P, Fieschi F (2006). Small-angle X-ray scattering reveals an extended organization for the autoinhibitory resting state of the p47(phox) modular protein. *Biochemistry* 45: 7185–7193.
- Heyworth PG, Curnutte JT, Nauseef WM, Volpp BD, Pearson DW, Rosen H *et al.* (1991). Neutrophil nicotinamide adenine dinucleotide phosphate oxidase assembly. Translocation of p47-phox and p67-phox requires interaction between p47-phox and cytochrome b558. *J Clin Invest* 87: 352–356.
- Jaquet V, Scapozza L, Clark RA, Krause KH, Lambeth JD (2009). Small-molecule NOX inhibitors: ROS-generating NADPH oxidases as therapeutic targets. *Antioxid Redox Signal* 11: 2535–2552.
- Jault JM, Fieulaine S, Nessler S, Gonzalo P, Di Pietro A, Deutscher J *et al.* (2000). The HPr kinase from *Bacillus subtilis* is a homo-oligomeric enzyme which exhibits strong positive cooperativity for nucleotide and fructose 1,6-bisphosphate binding. *J Biol Chem* 275: 1773–1780.
- Ji SM, Wang QW, Chen JS, Sha GZ, Liu ZH, Li LS (2006). Clinical trial of *Tripterygium Wilfordii* Hook F. in human kidney transplantation in China. *Transplant Proc* 38: 1274–1279.
- Kiaei M, Kipiani K, Petri S, Chen J, Calingasan NY, Beal MF (2005). Celastrol blocks neuronal cell death and extends life in transgenic mouse model of amyotrophic lateral sclerosis. *Neurodegener Dis* 2: 246–254.
- Kim Y, Kim K, Lee H, Han S, Lee YS, Choe J *et al.* (2009). Celastrol binds to ERK and inhibits FcεpsilonRI signaling to exert an anti-allergic effect. *Eur J Pharmacol* 612: 131–142.
- Kuhns DB, Alvord WG, Heller T, Feld JJ, Pike KM, Marciano BE *et al.* (2010). Residual NADPH oxidase and survival in chronic granulomatous disease. *N Engl J Med* 363: 2600–2610.
- Kume A, Dinauer MC (2000). Gene therapy for chronic granulomatous disease. *J Lab Clin Med* 135: 122–128.
- Lambeth JD, Krause KH, Clark RA (2008). NOX enzymes as novel targets for drug development. *Semin Immunopathol* 30: 339–363.
- Lew M (2007). Good statistical practice in pharmacology. *Problem 2. Br J Pharmacol* 152: 299–303.
- Li Y, Trush MA (1998). Diphenylethylidenehydrazide, an NAD(P)H oxidase inhibitor, also potently inhibits mitochondrial reactive oxygen species production. *Biochem Biophys Res Commun* 253: 295–299.
- Murphy BM, O'Neill AJ, Adrain C, Watson RW, Martin SJ (2003). The apoptosome pathway to caspase activation in primary human neutrophils exhibits dramatically reduced requirements for cytochrome C. *J Exp Med* 197: 625–632.
- Nauseef WM (2007). Isolation of human neutrophils from venous blood. *Methods Mol Biol* 412: 15–20.
- Nauseef WM, Volpp BD, McCormick S, Leidal KG, Clark RA (1991). Assembly of the neutrophil respiratory burst oxidase. Protein kinase C promotes cytoskeletal and membrane association of cytosolic oxidase components. *J Biol Chem* 266: 5911–5917.
- Nobuhisa I, Takeya R, Ogura K, Ueno N, Kohda D, Inagaki F *et al.* (2006). Activation of the superoxide-producing phagocyte NADPH oxidase requires co-operation between the tandem SH3 domains of p47phox in recognition of a polyproline type II helix and an adjacent alpha-helix of p22phox. *Biochem J* 396: 183–192.
- O'Donnell BV, Tew DG, Jones OT, England PJ (1993). Studies on the inhibitory mechanism of iodonium compounds with special reference to neutrophil NADPH oxidase. *Biochem J* 290 (Pt 1): 41–49.
- Peachman KK, Lyles DS, Bass DA (2001). Mitochondria in eosinophils: functional role in apoptosis but not respiration. *Proc Natl Acad Sci U S A* 98: 1717–1722.
- Salminen A, Lehtonen M, Paimela T, Kaarniranta K (2010). Celastrol: molecular targets of thunder god vine. *Biochem Biophys Res Commun* 394: 439–442.
- Serrander L, Cartier L, Bedard K, Banfi B, Lardy B, Plastre O *et al.* (2007a). NOX4 activity is determined by mRNA levels and reveals a unique pattern of ROS generation. *Biochem J* 406: 105–114.
- Serrander L, Jaquet V, Bedard K, Plastre O, Hartley O, Arnaudeau S *et al.* (2007b). NOX5 is expressed at the plasma membrane and generates superoxide in response to protein kinase C activation. *Biochimie* 89: 1159–1167.
- Sun H, Liu X, Xiong Q, Shikano S, Li M (2006). Chronic inhibition of cardiac Kir2.1 and HERG potassium channels by celastrol with dual effects on both ion conductivity and protein trafficking. *J Biol Chem* 281: 5877–5884.
- Suter DM, Cartier L, Bettiol E, Tirefort D, Jaconi ME, Dubois-Dauphin M *et al.* (2006). Rapid generation of stable transgenic embryonic stem cell lines using modular lentivectors. *Stem Cells* 24: 615–623.
- Swain SD, Helgersson SL, Davis AR, Nelson LK, Quinn MT (1997). Analysis of activation-induced conformational changes in p47phox using tryptophan fluorescence spectroscopy. *J Biol Chem* 272: 29502–29510.
- Tao XL, Sun Y, Dong Y, Xiao YL, Hu DW, Shi YP *et al.* (1989). A prospective, controlled, double-blind, cross-over study of *Tripterygium wilfordii* hook F in treatment of rheumatoid arthritis. *Chin Med J (Engl)* 102: 327–332.
- Wang J, Gines S, MacDonald ME, Gusella JF (2005). Reversal of a full-length mutant huntingtin neuronal cell phenotype by chemical inhibitors of polyglutamine-mediated aggregation. *BMC Neurosci* 6: 1.

Wu F, Han M, Wilson JX (2009). Tripterine prevents endothelial barrier dysfunction by inhibiting endogenous peroxynitrite formation. *Br J Pharmacol* 157: 1014–1023.

Yamamoto A, Kami K, Takeya R, Sumimoto H (2007). Interaction between the SH3 domains and C-terminal proline-rich region in NADPH oxidase organizer 1 (Noxo1). *Biochem Biophys Res Commun* 352: 560–565.

Yang H, Chen D, Cui QC, Yuan X, Dou QP (2006). Celastrol, a triterpene extracted from the Chinese "Thunder of God Vine," is a potent proteasome inhibitor and suppresses human prostate cancer growth in nude mice. *Cancer Res* 66: 4758–4765.

Zhang T, Hamza A, Cao X, Wang B, Yu S, Zhan CG *et al.* (2008). A novel Hsp90 inhibitor to disrupt Hsp90/Cdc37 complex against pancreatic cancer cells. *Mol Cancer Ther* 7: 162–170.

Zhang T, Li Y, Yu Y, Zou P, Jiang Y, Sun D (2009). Characterization of celastrol to inhibit HSP90 and CDC37 interaction. *J Biol Chem* 284: 35381–35389.

Zhang Z, Marshall AG (1998). A universal algorithm for fast and automated charge state deconvolution of electrospray mass-to-charge ratio spectra. *J Am Soc Mass Spectrom* 9: 225–233.